IEEE Access
Multidisciplinary | Rapid Review | Open Access Journal

Date of publication xxxx 00, 0000, date of current version xxxx 00, 0000.

Digital Object Identifier 10.1109/ACCESS.2020.Doi Number

Time Stability of Untethered Electronic Switched MIMO Millimeter-Wave Channel Sounders

Ruoyu Sun[1], Senior Member, IEEE, Peter B. Papazian[2]

[1]Cable Television Laboratories, Louisville, CO 80027 USA
[2]National Institute of Standards and Technology, Boulder, CO 80305 USA

Corresponding author: Ruoyu Sun (e-mail: ruoyusun@ieee.org).

ABSTRACT Untethered channel sounders are used to measure mobile radio propagation channels. As high data rate, millimeter-wave and multiple-input multiple output (MIMO) are considered in the next generate communications systems, knowledge of the propagation channel needs to be studied in high accuracy. Measuring time stability of the clocks in both transmitter and receiver is essential when characterizing relative delay between multipath components (MPCs), absolute delay, angle of arrival (AoA) and angle of departure (AoD) of MPCs. This paper describes timing circuit design of untethered electronic switched MIMO millimeter-wave channel sounders, proposes practical method to remove a constant initial time error, and experimentally estimates time stability of the channel sounders. Time stability is classified in three categories: short-term (in order of microseconds) that impacts relative delay, AoA and AoD; medium-term (in order of minutes) that impacts absolute delay; and long-term stability (in order of days) that can be used to verify clock calibration and noise. This is the first time to apply standard parameters for measuring clock stability, such as timing Allan deviation (TDEV) and time interval error (TIE), to channel sounding and modeling. Novel methods are developed for measuring jitter and short-term noise. It was found that TDEV for short-term measurements was less than 1 ps and the medium-term timing errors due to clock noise could be maintained at 0.4 ns/min.

INDEX TERMS Time stability, synchronization, channel sounding, millimeter-wave

I. INTRODUCTION

Millimeter wave (mmW) spectrum has been identified by industry, and allocated by the Federal Communications Commission (FCC), for fifth-generation (5G) communication systems. These frequency bands will accommodate larger bandwidths, higher data rates and the lower latency required for the next generation systems. Because radio wave propagation is distinctly different at these radio frequencies many millimeter wave channel sounders have been developed [1-5]. Data from sounders are used to quantify radio wave propagation at millimeter wave frequencies and are used for the development of models and standards for 5G radio systems.

5G new radio requires new technology to operate at millimeter wave frequencies. High-gain and pencil-beam antenna arrays that can track multipath components (MPCs) are important to compensate high path loss [6]. To increase data rate, high bandwidth operation is required. These requirements lead to the need for more precise timing within systems. This is true for new channel sounders as well as new radio systems which will control phase and tracking using integrated radio frequency (RF) front-ends [7]. The National Institute of Standards and Technology (NIST) channel sounder which employed a switched antenna array, needs picosecond timing accuracy to measure angles of arrival (AoAs) and angles of departure (AoDs) of multipath signals. This requires not only precision oscillators and clocks, but also measurement methods to characterize their stability. The need for precision timing will increase as radio frequencies are pushed beyond 100 GHz to 300 GHz. Sounding systems are also being developed in this frequency range [8-9].

The NIST sounder relies on Rubidium (Rb) clocks for untethered operation and system synchronization over a

This article has been accepted for publication in a future issue of this journal, but has not been fully edited. Content may change prior to final publication. Citation information: DOI 10.1109/ACCESS.2020.2968355, IEEE Access

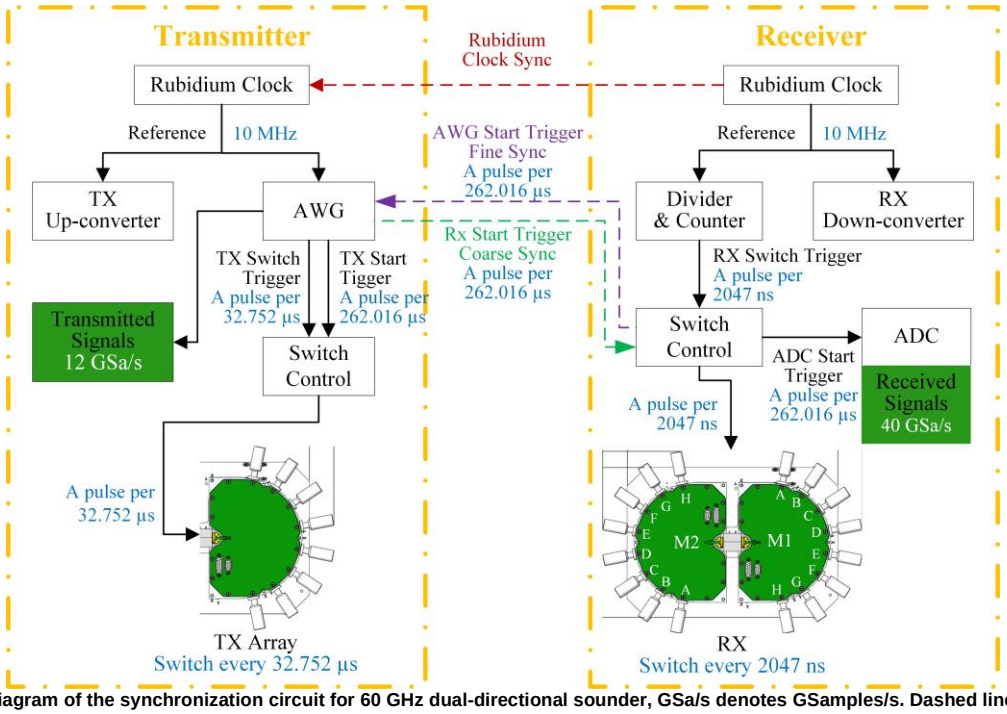

FIGURE 1. Block diagram of the synchronization circuit for 60 GHz dual-directional sounder, GSa/s denotes GSamples/s. Dashed lines (red, purple and green) are connecting cables that adjust the frequency of the slave Rb clock to a master Rb clock.

time-period of hours as required for measurement campaigns. It also relies on low phase noise oscillators for short-term timing. Short-term timing stability is necessary for synchronization of the sounder's antenna multiplexor, digitizer at the receiver, and local oscillator (LO) generation at both the transmitter and receiver. These signals needed picosecond stability but only for a period of one measurement cycle which is completed on a microsecond time scale. Consequently, the time intervals needed to characterize the timing instabilities are milliseconds to hours with below picosecond resolution.

When facing a system with timing errors which caused unacceptable AoA and AoD errors, we need to quantify the long- (hour to days), medium- (minutes) and short-term (microseconds) stability of its clocks and oscillators. The traditional method is to use a more accurate clock or oscillator as a reference. Then a time sequence of the phase or time differences between the clocks or oscillators is measured. These data can then be processed to yield both time and frequency domain timing metrics. For medium-term stability we were able to use the traditional method which employed a hydrogen maser available at NIST [10]. This allows us to measure the stability of the Rubidium clocks over periods of minutes to days.

There were multiple problems with this method when measuring short-term stability. First, one needs lower phase noise clocks and oscillators at the required measurement frequencies which were not available using the maser. Second, traditional phase meters cannot measure time stability over such short periods. Faced with these problems we developed novel methods to measure the short-term stability of the system which only required our system components. We characterized the time stability of the system when stationary and when moving in untethered mode.

Contributions of this paper includes presenting design of a channel sounder timing circuit; classifying sounder time stability in to three categories: short-term, medium-term and long-term stability; introducing statistical parameters used to characterize clock stability into field of channel sounding and designing a measurement method to quantify short-term stability; and experimentally estimating medium-term stability. The proposed methods will help engineers faced with similar problems to synchronize and quantify clock and oscillator performance for millimeter wave systems. It uses standard metrics developed by the NIST Time and Frequency Division [11-13] which are codified in an IEEE standard. Short-time scale methods developed for the sounder require only software and the system components. This allows calibrations of this critical metric when making field measurements.

The electronic switching and timing circuits as well as the timing error estimation method are not only limited to mmW bands, but also applicable to all frequencies. Higher frequencies require more high-gain and narrow-beam antennas to compensate high path loss, which increase complexity of the timing system. Additionally, mmW bands require higher temporal and angular resolutions and higher time stability to resolve richer reflections and MPCs in mmW bands.

The paper is organized as follows. A description of the system is presented in section II. Synchronization is

This article has been accepted for publication in a future issue of this journal, but has not been fully edited. Content may change prior to final publication. Citation information: DOI 10.1109/ACCESS.2020.2968355, IEEE Access

described in Section III. Short-term time stability (on the order of microseconds to milliseconds) is discussed in Section IV. This section is important because it effects the relative delay between MPCs as measured by different antenna elements. The relative delay is then used to estimate AoA and AoD of the MPCs. Medium-term stability is discussed in Section V. This medium-term stability affects the absolute delay of the channel impulse response (CIR) which is useful for comparing multipath tracking and AoA and AoD to ray tracing. In Section VI we conclude.

II. GUIDELINES FOR MANUSCRIPT PREPARATION

A. NIST CHANNEL SOUNDER

NIST designed three channel sounders at frequencies 28, 60, and 83 GHz. They transmit a pseudorandom bit sequence (PRBS). Correlation of the PRBS signal with the received signal yields the CIR. Such a system is often called a "correlation-based channel sounder."

In our system, the transmitter (TX) employs an arbitrary waveform generator (AWG) to generate a modulated intermediate frequency (IF) signal at 12 GSamples/s. The IF signal is then up-converted to RF and radiated by either an omnidirectional antenna or an electronically switched antenna array. The radiated signals are detected using an electronically switched antenna array and pre-amplified. They are then down-converted and sampled by a high-speed digitizer at 40 GSamples/s [14]. Phase-Locked Dielectric Resonator Oscillators (PLDROs) are employed as LOs for the up-/down-convertors. The IF signal is then converted to base band in software and correlation processing is used to generate the CIR of the channel.

The 28- and 83-GHz sounders transmit at 1 Gbits/s with an omni-directional TX antenna. The PRBS length is 2047 bits (or chips) in 2047 ns. The RX array utilize 16 horn antennas oriented on an octagon. The antennas are electronically switched on or off with an interval of two PRBS lengths of 4.094 μs, from which a directional CIR is recorded. Then 16 directional CIRs are combined to an omni-directional CIR with a measurement period of 65.504 μs.

The dual directional 60-GHz TX and receiver (RX) use the same timing system and synchronization as the 28- and 83-GHz sounders. The 60-GHz system transmits at 2 Gbits/s and utilizes eight directional horn antennas arranged on a semi-octagon. The eight transmit horns enable AoD measurements and increase gain and equivalent isotropically radiated power (EIRP). The TX antennas switch every RX rotation, where one rotation enables the recording of all RX antennas over a 360° scan. Only one pair of TX and RX antennas perform channel measurements at a time. For most environments, signals from all TX antennas are recorded by all the RX antennas during the channel coherence time due to the fast switching of the systems [15]. With these configurations, the RX antennas switch every two PRBS lengths of 2047 bits in 2.047 μs, from which a direction CIR is extracted. Then 16 × 8 = 128 directional CIRs are combined to an omni-directional CIR within 262.016 μs and include AoA and AoD data.

The AoA and AoD of MPCs are extracted using the space-alternating generalized expectation maximization (SAGE) algorithm [16-18]. MPCs can be extracted with delay resolution of up to 0.5 ns and AoA/AoD resolution of 1° [19]. For these estimates the short-term time stability is critical because the delay and amplitude of MPC's at multiple antennas are used by the SAGE algorithm. Relative time stability in ps needs to be maintained to maintain phase stability at 60 GHz while the arrays switch between TX and RX antennas.

The medium-term time stability for periods of minutes to hours determines the absolute time of flight between transmitter and receiver. For the study of Doppler time stability on the order of ms to several seconds is needed. Phase coherence of < 0.1 rad is considered for short-term time stability and is necessary for super-resolution MPC extraction. Both medium-term stability and phase coherence require accurate synchronization. The synchronization circuit block diagram for the 60 GHz dual directional sounder is illustrated in Fig. 1. Rb clocks are commonly used for synchronization of channel sounders. An example is given in [20]. Medium-term synchronization between the TX and RX rely on separate Rb clocks. These clocks provide 10-MHz reference signals for the AWG (TX), analog to digital converter (ADC, RX) and local oscillators which use PLDROs for both TX and RX.

Three coaxial cables are connected before the channel measurement for calibration, as the dashed lines shown in Figure 1. The red dashed line is used to sync two Rb clocks using the pulse per second (PPS) output of the receiver Rb as input to the transmitter Rb PPS input. This adjusts the Rb frequency at the transmitter to the receiver Rb. The frequency difference of the clocks determines the drift rate of the absolute timing circuit of the sounder as discussed further in Section IV. The purple and green dashed lines are for fine and coarse sync between timing circuit in TX and RX, see Section III. After synchronization, the TX and RX are untethered for mobile measurements.

In the RX timing circuit, the divider/counter is driven by a bit rate clock (not shown on diagram) which is run at the sounder TX bit rate and remain synchronized with the TX clocks by phased locking to the Rb clocks. A fast counter generates a pulse every two code words (switching rate for the antenna multiplexor). A logic level comparator circuit changes the analog code word trigger to a transistor-transistor logic (TTL) level signal. This switching signal is converted to a 4-bit digital IO signal and used to switch the RX antenna array. The TTL signal is further divided by the 16 (the number of RX antenna elements) for ADC triggering at integer numbers of rotations where one rotation means all the receive antennas have been switched and recorded in sequence.

This article has been accepted for publication in a future issue of this journal, but has not been fully edited. Content may change prior to final publication. Citation information: DOI 10.1109/ACCESS.2020.2968355, IEEE Access

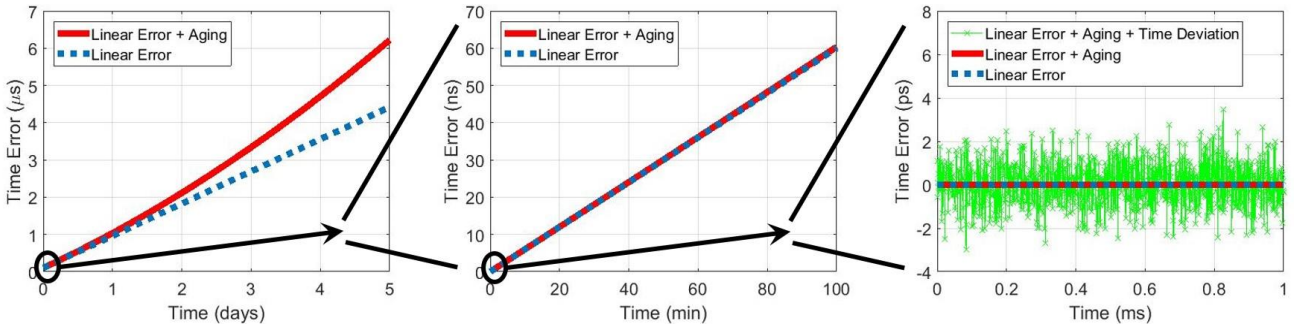

FIGURE 2. Time error over time in equation (1) with zero initial time error x_0; the frequency offset $\Delta f/f$ and drift D are 1×10^{-11} and 1.93×10^{-17}/s, respectively, according to the specifications of the Rubidium clocks, (a) long-term time stability: effects of aging (non-linear error) and frequency offset (linear error) for the time duration of days; (b) medium-term time stability: effects of frequency offset and aging for the time duration up to 100 minutes; (c) short-term time stability: effects of time deviation and frequency offset of time duration of one millisecond.

The TX timing circuit is simpler since the AWG not only generates the TX modulated signal but also creates two triggers: a switch trigger for the TX antennas and a start trigger for synchronization of digitizer records with TX generated code words.

B. COMPONENTS OF TIMING ERROR

The total time error between two clocks is, by convention, $x(t)$ and is measured as a time difference between transmitted and received waveforms. It can be predicted using

$$x(t) = x_0 + y_0 t + \frac{1}{2} D t^2 + \sigma_x(t), \qquad (1)$$

where x_0 denotes a constant initial time offset between two clocks, $y_0 = \Delta f/f$ is a constant fractional-frequency offset (sometimes called holdover); D denotes a constant linear frequency drift (sometimes called aging) caused by Rubidium clock noise; and $\sigma_x(t)$ is a random noise or environmentally-induced time deviation. Fig. 2(c) illustrates effects of short-term stability that is due to $\sigma_x(t)$.

The long-term (on the order of days or months) aging rate timing error is given by $\frac{1}{2} D t^2$ in (1), as shown in Fig. 2(a). Since the two Rb clocks in the NIST channel sounders are synchronized before the measurements and the measurements only last for a few hours. Time error related to drift is negligible.

The medium-term stability is shown in Fig. 2(b), where the slope of the linear error (blue dashed line) is also called holdover. Holdover is a fractional frequency specification reported for a 24-hour period, which derives from $y_0 = \Delta f/f = -\Delta t/24\ hours$ on most clock specification sheets. Alternatively, on some clocks, it is the "holdover, Stratum 1 level." For the Rb clocks used in our tests the holdover specification is 10^{-11} for 24 hours and is used to predict stability of the absolute time of arrival for typical field measurement periods.

The traditional method for measuring time stability is to evaluate $y_0 t + \frac{1}{2} D t^2$ in equation (1) with a more accurate clock by measuring the phase difference between the clock-under-test and the reference clock over time.

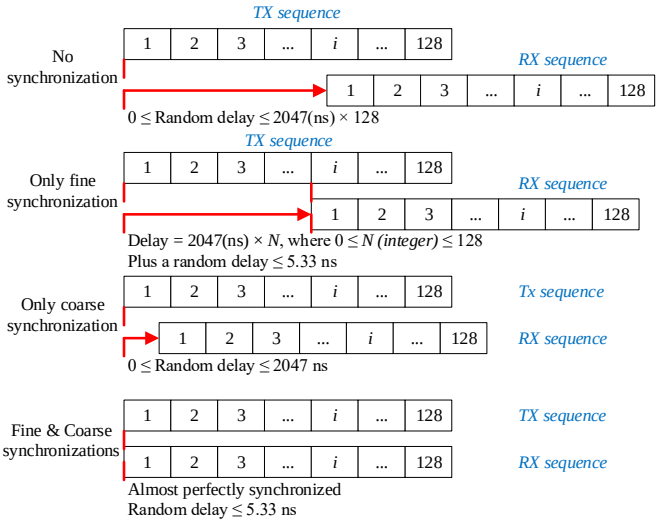

FIGURE 3. Effects of fine and coarse synchronizations, which remove the initial synchronization error T_0 in (1).

The remaining sections deal with methods for estimating the initial time offset (x_0 in (1)), time stability when the system is moving ($y_0 t$ in (1)) and short-term oscillator performance ($\sigma_x(t)$ in (1)). The former two affect estimates of time-of-arrival, while the latter affects the accuracy of AoA and AoD estimates derived from our system. We developed new methods to measure these quantities.

III. INITIAL TIME OFFSET

Since clocks and triggers in TX and RX start at a random time, a constant initial time error, T_0, exists between TX and RX. This constant error changes once any component in the timing circuit powered off/on. To eliminate the initial synchronization error T_0, both coarse sync and fine sync are implemented using the trigger lines shown in Figure 1.. The effects of coarse and fine synchronization are shown in Fig. 3. The delay is a random value without any synchronization between the TX and RX.

To address synchronization, in an initialization step before field tests, the AWG provides start triggers for both the TX

This article has been accepted for publication in a future issue of this journal, but has not been fully edited. Content may change prior to final publication. Citation information: DOI 10.1109/ACCESS.2020.2968355, IEEE Access

and the RX, termed coarse sync (see Fig. 3). This synchronization is maintained by the Rb clock after the initialization step, allowing disconnection of the TX and RX. The coarse sync reduces the random delay to within a single PRBS sequence, 2047 ns.

However, the AWG in the TX and the antenna switch control module in the RX start at random times relative to each other, which introduces a random delay between zero and 2047 ns. Because the antenna switch control module at the receiver outputs a pulse every 2047 ns, we initialize the trigger in the AWG with pulses from the switch control module to remove this random delay. This "fine sync," also shown in Fig. 3, is accomplished through direct connection of the switch control module to the AWG prior to each field test.

In other words, the coarse sync aligns the indices (but not boundaries) of the TX and RX antenna switching time slots and the fine sync aligns the boundaries (but not indices). Combination of coarse and fine synchronizations provides the required performance.

IV. SHORT-TERM TIME STABILITY

The NIST mmW channel sounders utilize large bandwidth of 1 or 2 GHz with sampling rate of 40 GSamples/s (25 ps per sample). Bandwidth is essential to resolve relative delay, AoAs and AoDs of MPCs, such as the RMS delay spread achieves 0.1 ns level in [6] and angular resolution achieves one-degree level [19]. Another key parameter to achieve such high resolutions is the jitter of the sounder. The jitter needs to be much smaller than the delay resolution or 25 ps sampling interval. Short-term stability estimates magnitude of the jitter.

Sources in channel sounder that introduce noise and hence degrade time stability include

i. LO sources (PLDROs) (in both TX and RX)
ii. clock inside AWG (at the TX)
iii. clock inside ADC (at the RX)
iv. divider/counter and switch control in timing circuit;
v. frequency differences between two Rb clocks (drift and frequency offset).

As we will show, short-term stability is affected by sources i-iv and long-/medium-term stability is determined by source v. Note that our evaluation of the short-term stability is at a system level that cannot separate effects from sources ii and iii based on the equipment and metrology used in this study.

A. MEASUREMENT METHOD AND RESULTS

The short-term time stability is evaluated through a conducted setup, as shown in Fig. 4. There are two clock modes: a common single clock and 2 independent clocks. A continuous wave (CW) signal is employed, which allows evaluation of short-term time stability using zero crossing time offsets. As we will show, the time stability is mainly affected by the frequency variation/phase noise of the PLDROs and the noise in the AWG and digitizer clocks. This noise is independent of bandwidth and can be related to the center frequency of the received signal.

A CW signal is generated at the IF with the AWG at 12 GSamples/s, and up-converted to RF. This signal propagated through the conducted "back-to-back"[1] (B2B) setup shown in Fig. 4, (composed of three waveguide sections and two adjustable attenuators). The signal is down-converted to IF, and digitized by the analog-to-digital converter (ADC) at 40 GSamples/s. An example measured sinusoid waveform is illustrated in Fig. 5 (red curve), which is compared to an ideal sinusoid signal created in software (blue curve). The zero-crossing points of measured signal $t_{m,i}$ and ideal signal $t_{i,i}$ (green points in Fig. 5) are compared, where i denotes index of timing points or samples. Their difference may be given by

$$x_i' = t_{m,i} - t_{i,i}. \tag{2}$$

The average of x_i' is a random number but only zero-mean jitter $\sigma_x(t)$ is of interest. By subtracting average of x_i' from x_i', we have:

$$x_i = x_i' - \frac{1}{L}\sum_{i=1}^{L} x_i', \tag{3}$$

where L denotes the number of samples of x_i or x_i'. The root-mean square (RMS) variation of x_i is commonly called "jitter" and estimates the time stability of the measured signal for short intervals [21].

The ADC digitizes the CW signal with a sample interval of 25 ps. To improve the estimate of the zero-crossing point $t_{m,i}$, the measured waveform is linearly interpolated by a factor of 100 to better identify zero crossing points. Limited by the memory size of the digitizer, we collected 20 ms of data for this study. The CW waveform's period τ_0 was 400 ps at 2.5-GHz IF for the 28 GHz system, 333 ps at 3-GHz IF for the 60 GHz system and 200 ps at 5-GHz IF for the 83 GHz system. To reduce the number of calculations, one thousandth of the zero-crossing points were used. As a result, the length of vector $t_{m,i}$ (and hence x_i) was 50,000 at 2.5 GHz (60,000 at 3 GHz and 100,000 at 5 GHz). After the decimation, the time interval τ between x_i and x_{i+1} is 400 ns at 2.5 GHz, 333 ns at 3 GHz and 200 ns at 5 GHz. These parameters are listed in Table I.

[1] Back to back refers to a common practice used when calibration channel sounders. It requires removing the antennas and connecting the transmitter to the receiver using a perfect channel such as a coaxial cable or wave guide to perform the calibration of the transceiver. If the antennas cannot be removed then this step can be accomplished using an anechoic chamber.

This article has been accepted for publication in a future issue of this journal, but has not been fully edited. Content may change prior to final publication. Citation information: DOI 10.1109/ACCESS.2020.2968355, IEEE Access

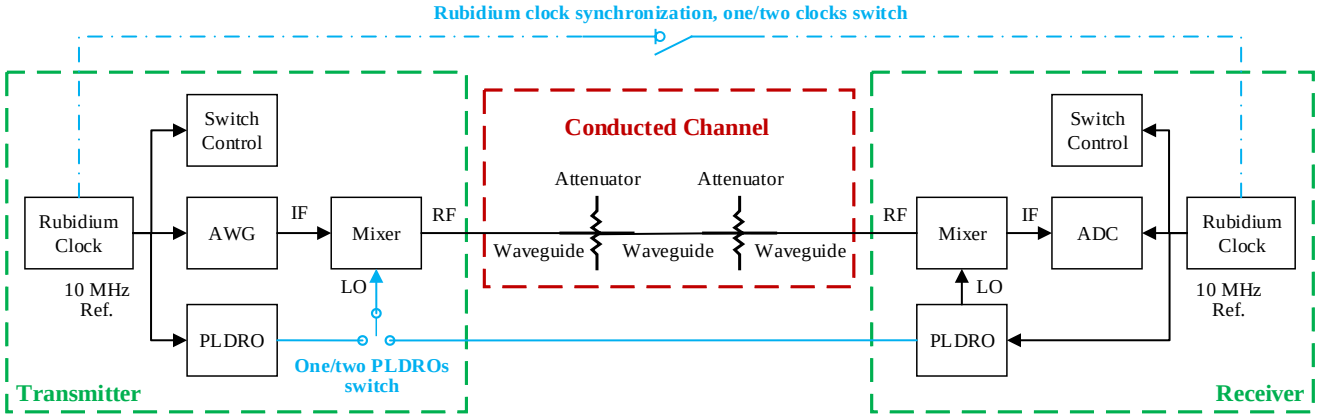

FIGURE 4. Block diagram of B2B setup, Rubidium clocks and PLDROs. Note that amplifiers, filters, isolators and many other RF components are ignored in this diagram.

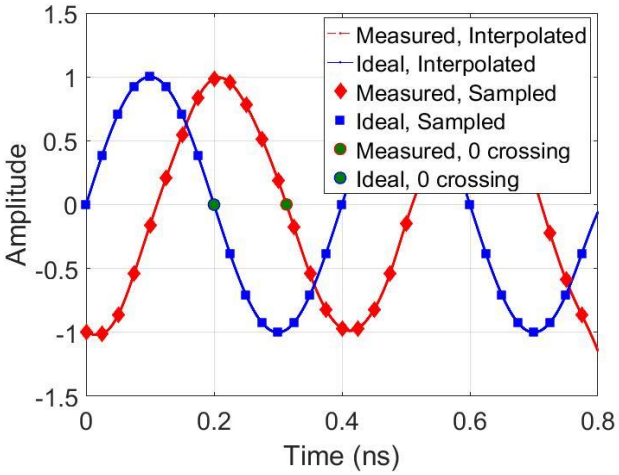

FIGURE 5. Waveform and zero crossing points for measured and ideal signals at 28 GHz.

To assess the effects on short-term timing stability of the Rb clocks, PLDROs and sources ii-iv listed in above, multiple test cases were conducted, as listed in Table II. Our evaluation tests include 1 (common) or 2 (independent) clocks, 1 or 2 PLDROs and an IF direct case in which the IF signal was transferred from AWG to ADC, without the up- and down-converters. These test cases were selected because we had PLDROs from two different manufacturers, one for the 83.5 GHz sounder and one for the 28.5 and 60.5 GHz sounders. We found the PLDROs from Manufacturer 1 had much better short-term stability statistics and replaced the PLDROs in 28.5 GHz and 60.5 GHz sounders with the PLDROs from Manufacturer 1. In follow-on tests, the tests were repeated using Manufacturer 1's PLDROs at 28.5 and 60.5 GHz to confirm the performance.

1) TIMING ERRORS FROM SOURCE I – RUBIDIUM CLOCKS

With the setup in Fig. 4, we could use either one common Rb clock split between the TX and RX or two Rb clocks separately as frequency references for the PLDROs. Example measurement results of x_i from (3) versus time are shown in Fig. 6. Fig. 6(a) plots the time difference over the

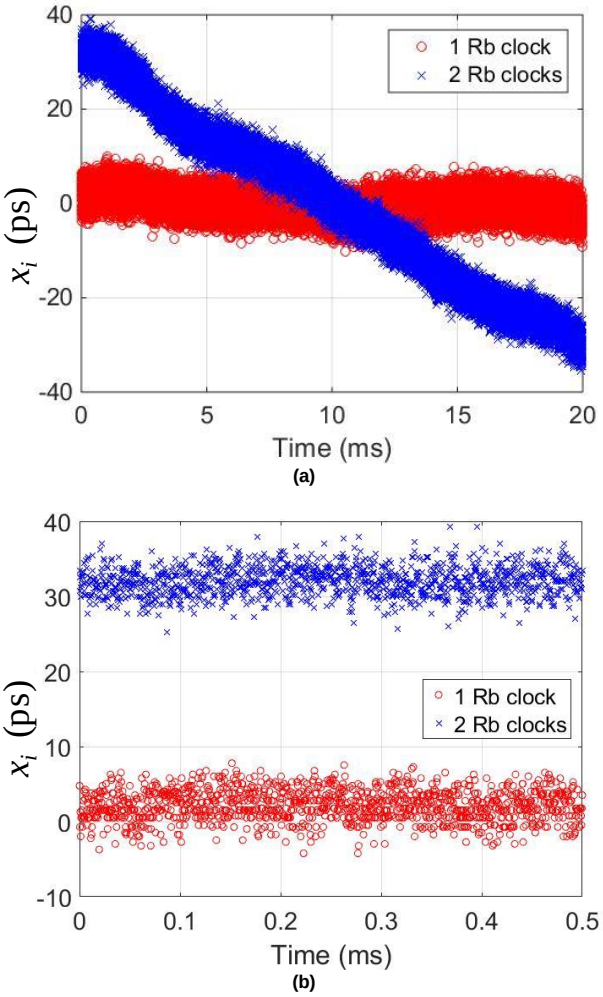

FIGURE 6. Example x_i over time for 28-GHz sounder with two PLDROs from Manufacturer 1: (a) over 20 ms; and (b) over the first 0.5 ms in (a).

duration of 20 ms, while Fig. 6(b) plots the time difference over 0.5 ms after the average slope of the time difference on the blue curve is subtracted. The blue band in Fig. 6(a) decreases over time, although it may increase or decrease depending on the sign of the frequency offset of the clocks

This article has been accepted for publication in a future issue of this journal, but has not been fully edited. Content may change prior to final publication. Citation information: DOI 10.1109/ACCESS.2020.2968355, IEEE Access

TABLE I
BASIC PARAMETERS FOR TIME STABILITY CHECKING.

RF (GHz)	28.5	60.5	83.5
IF (GHz)	2.5	3	5
τ_0 (ps)	400	333	200
τ (ns)	400	333	200
Length L of Δt_i	100,000	60,000	50,000

TABLE II
TEST CASES, "Y" DENOTES YES AND "--" DENOTES NO.

PLDRO Manufacturer	1				2			
Number of PLDRO	1		2		1		2	
Number of Rb Clocks	1	2	1	2	1	2	1	2
28.5 GHz	--	--	--	Y	Y	Y	Y	Y
60.5 GHz	--	--	--	Y	Y	Y	Y	Y
83.5 GHz	Y	Y	Y	Y	--	--	--	--

And

Number of Rb Clocks	1	2
IF direct	Y	Y

after synchronization. The slope of the blue curve is due to the fractional frequency offset between two clocks $\Delta f/f$ (y_0 in equation (1)). The width of the curves is due to phase noise in the clocks and signal sources. In Fig. 6(b), as the zoomed-in version of Fig. 6(a), the blue band appears flat in time spans less than 0.5 ms. To compare the stability over the duration of all TX/RX antenna combinations, we use short-term instability in the time span from 2 to 262 μs. The blue and red bands have similar width (less than 20 ps). Thus, we conclude that the short-term instability of the Rb clocks is not significant when compared to other timing-error mechanisms.

2) TIMING ERRORS FROM SOURCE II – PLDROS

We again used the conducted setup in Fig. 4 to use either a single PLDRO split between the TX and RX, or separate PLDROs in each. We also studied the effects of the quality of the PLDROs on timing error. An example x_i versus time result for the 28 GHz channel sounder with one Rb clock and PLDROs from Manufacturer 2 is shown in Fig. 7. The red curve represents the case for two PLDROs. Due to poor short-term time stability and phase noise of the PLDROs from Manufacturer 2, the LO frequencies in the up-converter and down-converter are not identical, with both randomly changing over time.

We next used a splitter to connect the PLDRO in the RX to mixers in both TX and RX (refer to Fig. 4). Although the LO frequency is randomly changing, it is common to both TX and RX and, hence, the relative time stability is much improved (blue curve in Fig. 7).

Note that the variation range of x_i for two PLDROs from Manufacturer 1 (red curve in Fig. 6) is very similar to that for a single PLDRO from Manufacturer 1 (not shown) and a single PLDRO from Manufacturer 2 (see Fig. 7), which indicates that the short-term time stability for the PLDROs from Manufacturer 1 is sufficient and does not degrade our sounding system.

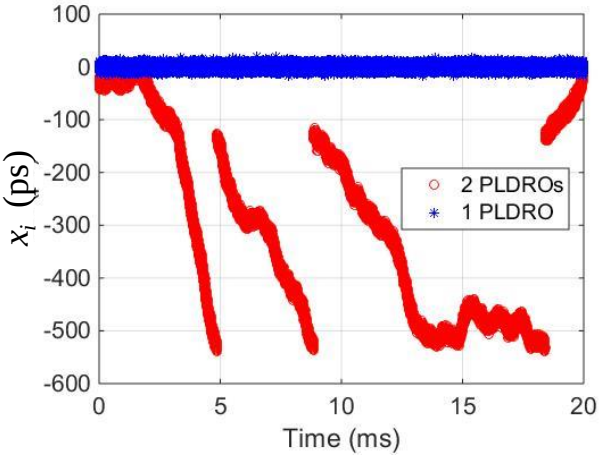

FIGURE 7. Example x_i over time for 28 GHz sounder with PLDROs from Manufacturer 2 and one Rubidium clock.

3) TIMING ERRORS, COUNTER AND SWITCH CONTROL SOURCE IV

We next performed the "IF direct" measurements in which the RF sections were omitted, and a cable connected the output of the AWG to the input of the RX at IF. The x_i versus time curve is very similar to the red one in Fig. 6. This indicates both that the x_i variation in Fig. 6 is due to the clocks driving the AWG and ADC, and also that the timing circuit (source iv) does not significantly degrade the system time stability.

B. STATISTICAL ANALYSIS

In this subsection, three statistical parameters are presented to quantitively analyze the results provided above. The square-root of the modified Allan variance is a common measure of frequency stability when measurement system noise dominates. Its primary use is to extract the underlying clock or oscillator stability from channel synchronization noise in this case. It is designed so that a few outlying phase "glitches" in the inner summation are smoothed (or suppressed) by the outer summation in (4) below. This variance is estimated from a set of M measurements for averaging time n as

$$Mod\sigma_y^2(\tau) = \frac{1}{2n^2\tau^2(M-3n+1)} \sum_{j=1}^{M-3n+1} \left\{ \sum_{i=j}^{j+n+1} [x_{i+2n} - 2x_{i+n} + x_i] \right\}^2. \quad (4)$$

The time Allan variance (TVAR) or its square root (time Allan deviation, TDEV) is a measure of time stability based on modified Allan variance [22-23] which could be directly used in (1)

This article has been accepted for publication in a future issue of this journal, but has not been fully edited. Content may change prior to final publication. Citation information: DOI 10.1109/ACCESS.2020.2968355, IEEE Access

$$\sigma_x^2(\tau) = \frac{\tau^2}{3} Mod\sigma_y^2(\tau). \quad (5)$$

The maximum time interval error (MTIE) and root-square mean time interval error TIE_{RMS} are time-stability measures commonly used in the telecom industry. TIE_{RMS} is the total RMS timing error over a time interval, including synchronization noise. Thus, glitches in sync are captured and are not distinguished from clock or oscillator random noise.

$$TIE_{RMS}(\tau) = \sqrt{\frac{1}{N-n}\sum_{i=1}^{N-n}(x_{i+n} - x_i)^2}, \quad (6)$$

where N denotes the number of data points (length of Δx_i); n is the number of data points in each time interval that ranges from 1 to N - 1; and time interval $\tau = n \times \tau_0$. TIE_{RMS} is similar to the standard deviation of x_i if there were no frequency offset. If frequency offset is present, TIE_{RMS} is a function of τ that measures time stability over a short time duration, while standard deviation is a statistic of the entire data set which makes no sense if x_i does not at least follow a Gaussian distribution.

MTIE quantifies the maximum time error over a particular time interval, which is very sensitive to a single extreme value. It is given by

$$MTIE(\tau) = \mathrm{Max}_{k\le i\le N-n}\{\mathrm{Max}_{k\le i\le k+n}(x_i) - \mathrm{Min}_{k\le i\le k+n}(x_i)\}. \quad (7)$$

MTIE measures the worst-case time interval error over the entire data set.

For the test cases listed in Table II, the time stability results, we include *TDEV*, TIE_{RMS} and *MTIE* for the three systems that are described in Table III. Again, our single-input, multiple-output sounders (SIMO) at 28 GHz and 83 GHz switch between RX antennas every 4.094 μs and a full RX array rotation is carried out in 65.5 μs. The multiple-input, multiple-output (MIMO) 60 GHz sounder switches between RX antennas every 2.047 μs, between TX antennas every 32.752 μs, and a full TX array rotation is carried out in 262.016 μs. We primarily consider these time interval values when evaluation timing stability of the switched array sounders for AoA and AoD measurements.

The results based on the use of one Rubidium clock and two Rubidium clocks are essentially similar, which indicates that the drift between Rubidium clocks does not affect the short-term stability over the duration of an antenna switch/rotation. The time stability statistics for the IF direct configuration at 2.5 GHz are close to the results with one PLDRO. This is primarily due to the clocks in the AWG and ADC (sources ii and iii). The results of two PLDROs from

TABLE III
SHORT-TERM TIME STABILITY STATISTICS

	Sounders	Time interval (μs)		1 Rubidium Clock			2 Rubidium Clocks		
				TIE_{RMS} (ps)	MTIE (ps)	TDEV (ps)	TIE_{RMS} (ps)	MTIE (ps)	TDEV (ps)
2 PLDROs	83 GHz Manufacturer 1	RX Switch	4.094	2.93	24	0.82	2.96	22.75	0.81
		RX Rotation	65.504	3.22	26.5	0.44	3.23	27	0.4
	60 GHz Manufacturer 2	RX Switch	2.047	50.55	344.25	19.92	58.62	343	22.77
		RX Rotation	32.752	53.12	344.25	12.98	60.28	343	13.94
		Full TX & RX Rotation	262.016	102.87	344.5	41.14	118.13	343	47.34
	60 GHz Manufacturer 1	RX Switch	2.047	2.36	9.75	0.73	2.27	11.76	0.71
		RX Rotation	32.752	2.93	15.00	0.60	2.87	15.50	0.61
		Full TX & RX Rotation	262.016	3.02	16.50	0.34	3.45	17.75	0.38
	28 GHz Manufacturer 2	RX Switch	4.094	40.54	415.25	8.46	65.77	414.5	13.96
		RX Rotation	65.504	50.13	415.5	12.29	76.64	415	15.57
	28 GHz Manufacturer 1	RX Switch	4.094	2.81	13.50	0.71	2.68	13.25	0.69
		RX Rotation	65.504	2.85	14.75	0.28	2.73	15.00	0.30
1 PLDRO	83 GHz	RX Switch	4.094	4.64	34.5	0.86	4.7	32.5	0.86
		RX Rotation	65.504	4.69	42	0.57	4.71	40.25	0.45
	60 GHz	RX Switch	2.047	3.44	16.75	0.92	3.35	17	0.9
		RX Rotation	32.752	3.44	17.25	0.26	3.34	19	0.25
		Full TX & RX Rotation	262.016	3.46	18.75	0.18	3.37	19.5	0.19
	28 GHz	RX Switch	4.094	6	28.75	1.28	5.63	27.25	1.22
		RX Rotation	65.504	5.98	31.5	0.35	5.62	31.5	0.35
IF direct at 2.5 GHz		SIMO RX Switch	2.047	2.82	20	0.8	2.83	20.25	0.77
		MIMO RX Switch	4.094	2.93	24	0.82	2.96	22.75	0.81
		SIMO RX Rotation	32.752	3.2	26.5	0.57	3.18	27	0.56
		MIMO RX Rotation	65.504	3.22	26.5	0.44	3.23	27	0.4
		MIMO Entire TX & RX Rotation	262.016	3.23	27.5	0.27	3.22	29.25	0.3

This article has been accepted for publication in a future issue of this journal, but has not been fully edited. Content may change prior to final publication. Citation information: DOI 10.1109/ACCESS.2020.2968355, IEEE Access

Manufacturer 2 are much worse than others, which concludes that PLDRO frequency drift could critically degrade short-term time stability.

Ultimately, we utilized PLDROs from Manufacturer 1. The field measurement systems utilize two PLDROs and two Rubidium clocks. The red-color values in Table III are the short-term time stability results corresponding to our channel sounders. The Modified Allan Deviation $\sigma_x(\tau)$ is smaller than 1 ps; TIE_{RMS} is smaller than 3.5 ps; and *MTIE* is less than 27 ps for all cases. They are all about two orders of magnitude smaller than the delay resolution of 0.5 ns for the 60 GHz sounder and 1 ns for the 28 and 83 GHz sounders.

The short-term stability does not significantly vary over three frequencies of 28, 60 and 83 GHz. This is because the clocks and timing circuit are the same among the three sounders. The only difference is PLDROs generating LO signals with different frequencies. As long as PLDROs are from the same manufacturer and have similar specifications, the time stability at 28, 60 and 83 GHz are very similar.

V. MEDIUM-TERM STABILITY (ORDER OF 1 TO 100 MINS)

The medium-term stability is due to the holdover of Rubidium clocks. It can be corrected by connecting a cable between Rb clocks in TX and RX. On the other hand, such a tethered sounder setting disables mobility. This Section only discusses untethered sounder setting where medium-term stability is not negligible.

The medium-term stability of the Rubidium frequency references is evaluated using a NIST hydrogen maser. This is using the traditional method as the maser is two orders of magnitude more stable than a Rb clock. These data are shown in Fig. 8. The period between 1 and 100 seconds on this graph is dominated by white noise, which yields a slope of -1 seen on the left on the log-log scale noise in the measurement. At approximately 600 seconds, the frequency stability of the clock has a minimum at 10^{-12}. After 1000 seconds, the Allan deviation begins to increase due to frequency drift. This is because the clock frequency drift and aging rate begin to affect the frequency stability. We see the frequency stability remains below 10^{-11} until the maximum measurement period of around 11,000 seconds (around three hours). This is the time stability holdover (y_0 in formula (1)). For this clock, the holdover remains below the clock specification for times longer than normal field measurement periods of about 3 hours.

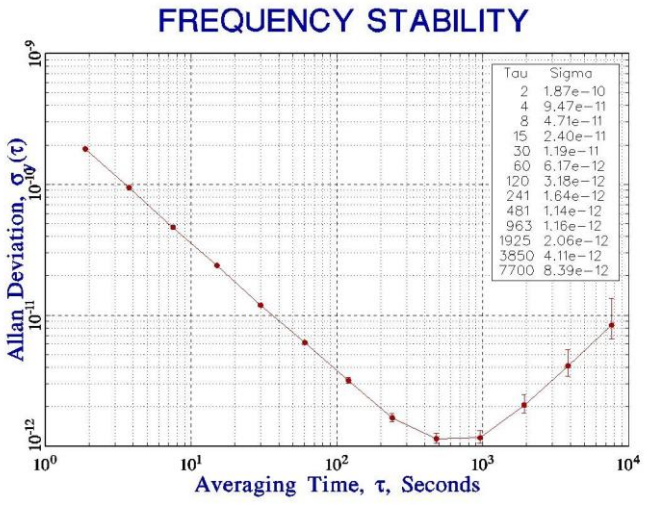

FIGURE 8. Allan deviation measurement data used for medium-term stability analysis of the rubidium system clock.

A measurement in our laboratory was conducted to evaluate the medium-term time stability of our channel sounder when in motion using a robotic platform. The path for this data is shown in Fig. 9(a). The transmitter was fixed at P = 1 m and Q = 1 m with height of 2.5 m above ground. The receiver on the robot was moving along a zig-zag pattern with an antenna height of 1.6 m. A line-of-sight condition was present during the entire measurement and the RX was in the far field. In total, 128 snapshots were recorded in 231.5 seconds. The robot accelerated in straight or curved lines in the zig-zag pattern reaching a maximum velocity of 0.72 m/s. It then stopped and turned the corners. Data were not collected when the velocity was below 0.05 m/s. The robot velocity over time is plotted in Fig. 9(c) and RF data were collected at 83 GHz along this path. Since the medium-term timing error is due to the two Rubidium clocks, the same medium-term timing error is expected for the other two sounder operating at 60 and 28 GHz with similar clocks.

Power delay profiles (PDPs, magnitude square of CIRs) were calculated from the measured data, from which the absolutely delay of the direct path (line-of-sight) was extracted, termed as measured delay x_m. The P and Q positions of the RX were recorded by the robot, as shown in Fig. 9(a). Hence, the "ground truth" time of flight x_g could be calculated. We estimated the medium-term timing error by comparing x_m and x_g as

$$\Delta x_j' = x_{g,j} - x_{m,j}, \tag{8}$$

and

$$\Delta x_j = \Delta x_j' - \Delta x_1', \tag{9}$$

where j denotes PDP index ranges from 1 to 128. The medium-term timing error x'_j over time is presented in Fig. 9(d). As discussed in Section II, the medium-term timing error is mainly due to fluctuations in the second term in equation (1) not being constant. For mobile measurements such as these, the environment-induced fluctuations of fractional frequency offset, $\Delta f/f$, is affected by acceleration/deceleration, rotation, or other physical movement. Such movements may impart more pressure on the quartz crystal that is phase-locked to the Rubidium cell. This can change the phase noise and frequency offset of the non-stationary (moving) system as compared to the

This article has been accepted for publication in a future issue of this journal, but has not been fully edited. Content may change prior to final publication. Citation information: DOI 10.1109/ACCESS.2020.2968355, IEEE Access

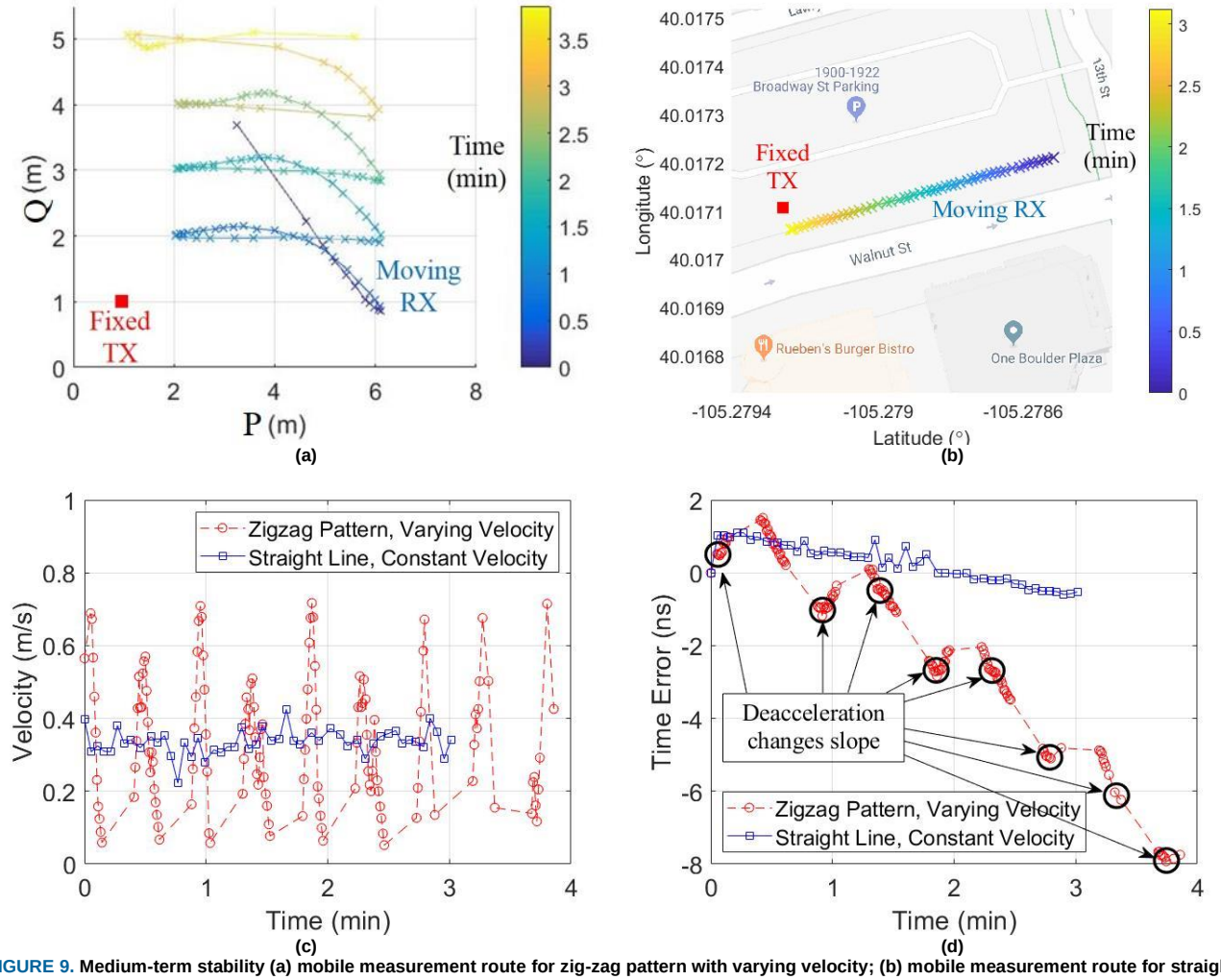

FIGURE 9. Medium-term stability (a) mobile measurement route for zig-zag pattern with varying velocity; (b) mobile measurement route for straight line patter with constant velocity; (c) velocity over time for two moving patterns; (d) medium-term timing error as a function of time for two moving patterns.

stationary (fixed-position) case.

The multiple straight red lines in Fig. 9(d), illustrate slope changes with sudden deacceleration that we observed. Other environment-induced effects could also change the slope, such as acceleration or rotation. These effects were not observed because the RX did not collect data when then velocity was less than 50 mm/s.

Based on the manufacturer's specifications of the Rubidium clocks that we used, the frequency offset of $\Delta f/f < 10^{-11}$ would induce a timing error of approximately 0.6 ns/min. Since we have two Rb clocks that may be drifting in opposite directions, the maximum frequency offset would be estimated as approximately 1.2 ns/min. However, this frequency offset is likely an underestimate due to following two reasons: 1) it does not consider the environment changes; and 2) the manufacturer's specifications are measured on the order of hours, a time scale that is significantly different from our channel sounding applications, which are on the order of minutes. Taking the measured time error difference of approximately 9.4 ns between the maximum and the minimum values in Fig. 9(d), and dividing this by the measurement's time duration of 231.5 s, we estimate the timing drift due to frequency offset to be approximately 2.45 ns/min. This means the absolute delay in PDPs could drift by as much as 2.45 ns within a one-minute measurement duration for this type of path.

The ground truth time of flight x_g may be used to circularly shift the PDPs to correct the absolute delay x_m, but this method is only valid in line-of-sight conditions. While this presents difficulty in establishing the absolute delay for the PDP, the medium-term timing error does not influence many other channel characteristics including the AoA/AoD, path loss, fading, delay spread and so on, as they are not dependent on the absolute delay. It can cause problems when analyzing the performance of tracking algorithms using ray tracing.

To further investigate this issue, absolute timing errors were measured when the robot was moving at a constant velocity and heading. An outdoor measurement was conducted in downtown Boulder, Colorado. As shown in Fig. 9(b), TX was fixed and RX was moving along a straight line with constant

This article has been accepted for publication in a future issue of this journal, but has not been fully edited. Content may change prior to final publication. Citation information: DOI 10.1109/ACCESS.2020.2968355, IEEE Access

velocity. The results are presented as the blue square symbols in Fig. 9(c) and (d). By minimizing acceleration and deacceleration the time of flight error was reduced to 0.4 ns per minute and had much less variability. To eliminate time of flight errors, the slope of the timing drift is measured and used to correct the data. The resulting correction is accurate to sub ns given the ps sampling period of the digitizer. As shown on Figure 8 the Allan Deviation of the Rb clock is below 10^{-11} for 10,000 s. This indicates the clock drift will be linear over field measurement time periods.

VI. CONCLUSION

AoA/AoD extraction and multipath tracking are critical parameters in the field of wireless propagation channel measurement and modeling, especially for mmWave and 5G applications. The short-term time stability of our channel sounders is fundamental for determining AoA/AoD and maintaining synchronization between antenna channels during fast antenna switching needed for the identifying multipath components. The medium-term timing errors due to frequency offsets between Rb clocks can be compensated for by measuring the relative timing drift between the two clocks and subtracting this term which remains linear during field measurements. In this paper, we first presented the synchronization/timing circuit design of our mmWave electronic switched MIMO channel sounders. We then discuss that the short-term timing error is caused by phase noise of local oscillators inside the up- and down-converters, and clocks in the AWG in the TX and in the ADC in the RX. We perform a set of conducted tests with or without the up- and down-converters, using three channel sounders at different radio frequencies, and with different local oscillator sources. We then generated statistics over the time intervals of our MIMO antenna switching. The time Allan Deviation was found to be lower than one picosecond for all cases. The maximum time interval error is lower than 27 ps.

The medium-term time error affects the absolute delay of MPCs in PDPs, and hence affects the MPC tracking. It is mainly due to the Rubidium clocks used for untethered operation. The medium-term time error is measured over-the-air in our lab and in the field under LOS conditions. The time of flight was compared using the geometry of the LOS path and delay of the direct path measured by the sounder. The slope of the medium- term drift for a zig-zag path is 2.45 ns /min., which is larger than the Rubidium clock manufacturer specifications of 1.2 ns/min. This is because the frequent acceleration and deacceleration of our positioning system induced additional changes of the of the fractional frequency offset between two clocks. This medium-term timing error could be removed if the TX and RX of a sounder are tethered and used identical clock sources, but then the user would lose the capability for mobile measurement. It was also found that by restricting sounder movement to low acceleration paths, the timing drift between the clocks could be reduced to 0.4 ns/min. Future work includes time stability analysis of global positioning system (GPS) based synchronization for sounders and massive MIMO phased array sounders.

REFERENCES

[1] R. Müller, R. Herrmann, D. A. Dupleich, C. Schneider and R. S. Thomä, "Ultrawideband multichannel sounding for mm-wave," *The 8th European Conference on Antennas and Propagation (EuCAP 2014), The Hague, pp. 817-821, 2014.*

[2] Zhu Wen *et al.*, "mmWave channel sounder based on COTS instruments for 5G and indoor channel measurement," *2016 IEEE Wireless Communications and Networking Conference Workshops (WCNCW)*, Doha, pp. 37-43, 2016.

[3] G. R. MacCartney, T. S. Rappaport, "A Flexible Millimeter-Wave Channel Sounder with Absolute Timing," *IEEE Journal on Selected Areas in Communications*, vol. 35, no. 6, pp. 1402-1418, June 2017.

[4] S. Salous, S. M. Feeney, X. Raimundo, A. A. Cheema, "Wideband MIMO Channel Sounder for Radio Measurements in the 60 GHz Band," *IEEE Transactions on Wireless Communications*, vol. 15, no. 4, pp. 2825-2832, April 2016.

[5] M. Peter, R. J. Weiler, W. Keusgen, T. Eichler, M. Kottkamp and A. Nähring, "Characterization of mm-wave channel sounders up to W-Band and validation of measurement results," *2016 10th European Conference on Antennas and Propagation (EuCAP)*, Davos, pp. 1-5, 2016.

[6] R. Sun *et al.*, "Millimeter-Wave Radio Channels vs. Synthetic Beamwidth," *IEEE Communications Magazine*, vol. 56, no. 12, pp. 53-59, December 2018.

[7] S..Kim, A. G. Zajić, "Statistical Characterization of 300-GHz Propagation on a Desktop," *IEEE Transactions on Vehicular Technology*, vol. 64, no. 8, pp. 3330-3338, Aug. 2015.

[8] S. Shinjo, K. Nakatani, K. Tsutsumi and H. Nakamizo, "Integrating the Front End: A Highly Integrated RF Front End for High-SHF Wide-Band Massive MIMO in 5G," *IEEE Microwave Magazine*, vol. 18, no. 5, pp. 31-40, July-Aug. 2017.

[9] S. Rey, J. M. Eckhardt, B. Peng, K. Guan and T. Kürner, "Channel sounding techniques for applications in THz communications: A first correlation-based channel sounder for ultra-wideband dynamic channel measurements at 300 GHz," *2017 9th International Congress on Ultra-Modern Telecommunications and Control Systems and Workshops (ICUMT)*, Munich, pp. 449-453, 2017.

[10] T. E. Parker, S. R. Jefferts and T. P. Heavner, "Medium-term frequency stability of hydrogen masers as measured by a cesium fountain," *2010 IEEE International Frequency Control Symposium*, Newport Beach, CA, 2010, pp. 318-323.

[11] IEEE 1139-2008 - IEEE Standard Definitions of Physical Quantities for Fundamental Frequency and Time Metrology--Random Instabilities, [Online] Available: https://standards.ieee.org/standard/1139-2008.html

[12] D. W. Allan, M.A. Weiss, J. L. Jespersen, "A frequency-domain view of time-domain characterization of clocks and time and frequency distribution systems," *Proc. 45th Freq. Cont. Symp.*, pp. 667-678, May 1991.

[13] W. J. Riley, "Handbook of Frequency Stability Analysis", *NIST Special Publication 1065*, pp19, July 2008.

[14] P. B. Papazian, C. Gentile, K. A. Remley, J. Senic and N. Golmie, "A Radio Channel Sounder for Mobile Millimeter-Wave Communications: System Implementation and Measurement Assessment," *IEEE Transactions on Microwave Theory and Techniques*, vol. 64, no. 9, pp. 2924-2932, Sept. 2016.

[15] P. B. Papazian *et al.*, "Calibration of millimeter-wave channel sounders for super-resolution multipath component extraction," *2016 10th European Conference on Antennas and Propagation (EuCAP)*, Davos, pp. 1-5, 2016.

[16] K. Hausmair, K. Witrisal, P. Meissner, C. Steiner, G. Kail, "SAGE algorithm for UWB channel parameter estimation," *COST 2100 Management Committee Meeting*, pp. 1-7. Feb. 2010.

[17] C. Gustafson, F. Tufvesson, S. Wyne, K. Haneda, and A. F. Molisch, "Directional analysis of measured 60 GHz indoor radio channels using SAGE", *IEEE Vehicular Technology Conf.*, pp. 1-5, May 2011.

[18] M. Choi, G. Grosskopf, D. Rohde, "Statistical characteristics of 60 GHz wideband indoor propagation channel," *IEEE Symp. on Personal, Indoor, Mobile Radio Communications*, pp. 1-5, Sept. 2005.
[19] R. Sun *et al*., "Design and calibration of a double-directional 60 GHz channel sounder for multipath component tracking," *2017 11th European Conference on Antennas and Propagation (EUCAP)*, Paris, pp. 3336-3340, 2017.
[20] J. Lee, M. Kim, J. Park, Y. Chong, "Field-Measurement-Based Received Power Analysis for Directional Beamforming Millimeter-Wave Systems: Effects of Beamwidth and Beam Misalignment," *ETRI Journal*, no. 40, Feb. 2018.
[21] D. A. Howe, T. N. Tasset, "Clock Jitter Estimation based on PM Noise Measurements," *Proc. 2003 Joint Mtg. IEEE Intl. Freq. Cont. Symp. and EFTF Conf.*, pp. 541-546, May 2013.
[22] D. A. Howe, D. W. Allan, J. A. Barnes, "Properties of Signal Sources and Measurement Methods," *Proc. 35th Ann. Symp. Freq. Control*, Philadelphia, PA, May 27-29, pp. A1-A47, 1981.
[23] D. B. Sullivan, D. W. Allan, D. A. Howe, F. L. Walls, "Characterization of Clocks and Oscillators," *NIST Tech. Note 1337*, pp. 1-342, 1990.

RUOYU SUN (M'13–SM'17) was born in Hohhot, China. He received the B.S. degree from Tianjin University in 2004, the M.S. degree from Beijing Jiaotong University in 2007, and the Ph.D. degree from the University of South Carolina in 2015, all in electrical engineering. His research interest includes radio propagation channel measurements and modeling and spectrum sharing.

Ruoyu is a Lead Architect at CableLabs, Louisville CO. From 2015 to 2018, he was an Electronics Engineer at NIST, Boulder CO, doing millimeter-wave channel sounder design, channel measurements and modeling. He worked at T3G Technology Co., Ltd, MOTOROLA and ST-Ericsson from 2007 to 2010 as a system integration test engineer working on TD-SCDMA/GSM/GRPS protocol and platforms. He has published over 50 articles, served on over 10 conference Technical Program Committees, reviewed over 180 manuscripts for academic journals and conferences.

PETER B. PAPAZIAN received his BS in Physics at SUNY Stonybrook in 1973 and an MS Degree from Colorado School of Mines in 1979. Currently, Peter is the 5G millimeter wave Channel Sounder project leader at the NIST Communications Technology Laboratory in Boulder, CO. The purpose of this research is to conduct millimeter wave Radio Channel propagation measurements to support model and standards development for 5G radio systems.